

Comparative study of the optical and economic performance of etendue-conserving compact linear Fresnel reflector concepts

A.E. Rungasamy, K.J. Craig* and J.P. Meyer

Department of Mechanical and Aeronautical Engineering, University of Pretoria, Pretoria 0002, South Africa.

*Corresponding author: ken.craig@up.ac.za

Abstract

This paper presents a comparative performance investigation of three Compact linear Fresnel collectors; a flat collector, a sun-tracking etendue-conserving collector and an off-peak etendue-conserving collector. A Monte Carlo ray tracing program is used to simulate the fields. The resultant incident radiation on the receiver aperture is used to quantify the geometric intercept factor and optical efficiency of the field. Each field is then optimised for mirror width and the ratio between the mirrors targeting each receiver aperture. The three fields are then compared on the basis of performance. The off-peak etendue-conserving compact linear Fresnel field reaches a peak geometric intercept factor of 92%, while the sun-tracking etendue-conserving field and flat field had a peak geometric intercept factor of 83% and 79% respectively. A maximum total plant cost for the same Levelized Electricity Cost is presented to incorporate a cost comparison.

Keywords: *etendue conserving; compact linear Fresnel; optimization; optical efficiency*

Nomenclature

Symbol	Definition	Symbol	Definition
δ	Significance factor	A_x	Position of mirror axes in x dimension
U	Etendue	A_y	Position of mirror axes in y dimension
R	Residual function	β	Mirror angle to the horizontal
α	Angle of the curve to the horizontal	γ	Geometric intercept factor
ϕ	Angle from a point to the receiver	\dot{Q}	Heat flux
θ	Incoming sun elevation angle, defined in East-West plane for mirror field aligned with North-South direction	η	Efficiency; subscript opt denote optical, th denotes thermal and pc denotes power cycle
H	Receiver height	G	Gap between mirrors
D	Domain width	λ	Cost
dl	Mirror width	ψ	Income
r	Mirror ratio	K	Cost of electricity per kW/hr
N_m	Number of mirrors; subscript S or M denotes single or multi-target		

1. Introduction

This paper sought to calculate and optimize the optical efficiencies of three conceptual designs for linear Fresnel collector fields (a flat compact linear Fresnel field and two etendue-conserving compact linear Fresnel fields) throughout the day. The one etendue-conserving design was a novel variant aimed at maximizing the off-peak performance, i.e., for non-vertical sun elevation angles.

Line focusing collectors are typically aligned from solar north to south, allowing for sun tracking to occur throughout the day about the mirror's primary axis of rotation as the sun travels from East to West. Linear Fresnel technology typically has a lower optical efficiency than parabolic trough technology, however the fact that it is significantly cheaper, has simpler manufacturing requirements and has lower wind loads makes the technology a desirable one (Ford, 2008). Muller et al. (2011) report that the capabilities of a standard linear Fresnel plant are comparable to that of a parabolic trough (see Table 1).

Table 1

Capabilities of typical parabolic trough and linear Fresnel plants (Muller et al, 2011)

	Capacity (MW)	Concentration	Peak solar efficiency (%)	Annual solar efficiency (%)	Thermal cycle efficiency (%)	Solar capacity factor (%)	Land use (m ² MW/hy)
Trough	10-200	70-80	21	10-15	30-40	25-70	6-8
Fresnel	10-200	25-100	20	9-11	30-40	25-70	4-6

Studies have therefore sought to increase the optical efficiency of linear Fresnel collectors by varying its configuration. Due to the discrete nature of the mirrors, adjacent mirrors can cause optical losses through blocking and shading. Eck et al. (2014) investigated the significance factor for optical losses to determine the influence of different losses on the annual electricity yield. The significance factor is defined in equation 1 as

$$\delta = \left| \frac{\Delta \text{yield} / \text{yield}}{\Delta \text{input} / \text{input}} \right| \quad (1)$$

The peak optical efficiency had the most significant effect on the annual electricity yield of the plant ($\delta = 0.88$), as compared to the Incidence angle modifier, end loss and shading significance factors of $\delta = 0.25$, $\delta = 0.01$ and $\delta = 0.06$ respectively. It is therefore of paramount importance to design the peak field with minimal losses.

Abbas et al. (2015) developed a set of equations to position mirrors far enough apart so that no blocking and shading would occur for a vertical sun elevation angle. Subsequently a number of studies sought to optimise the gap, mirror width and curvature of a standard linear Fresnel collector field. However, the effects of cosine losses due to the sun's changing altitude over the course of the day are much greater for linear Fresnel collector fields and it is therefore something that even an optimised linear Fresnel field cannot easily compensate for.

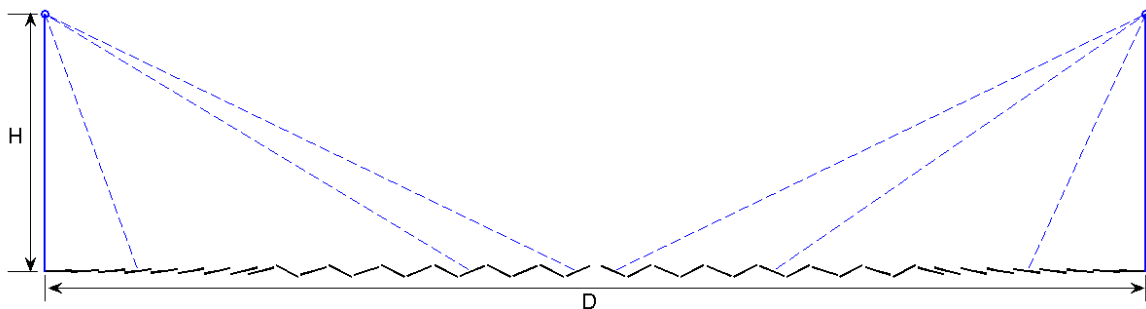


Fig. 1. Schematic of flat Compact linear Fresnel field (CLFR) for vertically incident sun rays

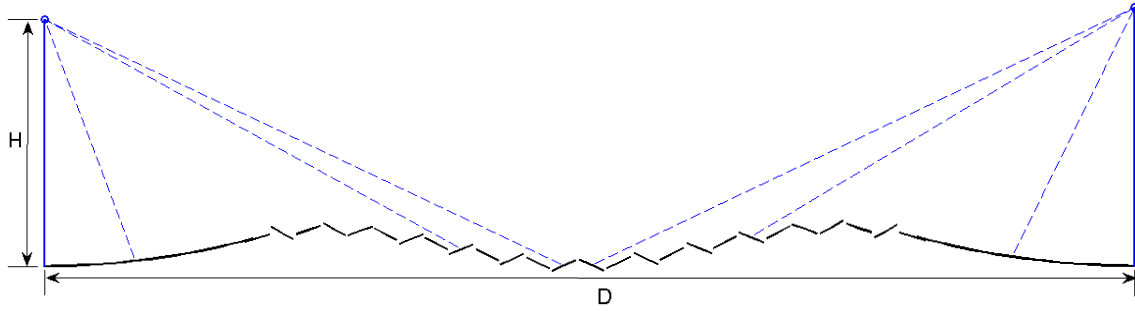


Fig. 2. Schematic of etendue-conserving Compact linear Fresnel field (ECCLFR) for vertically incident sun rays

Mills and Morrison (1999) proposed a compact linear Fresnel field (CLFR) with a minimum of two receivers, designed in such a way that the mirrors furthest from each receiver would alternate targets (Fig. 1). This created dissimilar target angles, allowing the mirrors to be placed closer together. This is due to the V type formation of the mirrors, which means that mirrors can be placed close together using only the required clearance gap as opposed to standard linear Fresnel mirrors that typically include a large gap to prevent blocking and shading between adjacent mirrors. The mirrors closest to each receiver would operate like a standard linear Fresnel field. This field represented a significant increase in optical efficiency.

In recent years, non-imaging optics concepts have been used to design collector fields. Chaves and Collares-Pereira (2010) introduced the concept of an etendue-conserving compact linear Fresnel field (ECCLFR), with mirrors placed along a curve (Fig. 2). Etendue is an effective measure of the "room" that light occupies in phase space, because as light travels it requires area and angular space (Chaves 2016). Etendue conservation is derived based on the law of conservation of energy. It stipulates that in a perfect optical system the etendue of the radiation through an entrance aperture must be equal to that of the radiation through an exit aperture. This describes an optical system in which no light rays are lost and designing a system where etendue is conserved is therefore analogous to designing a no-loss system or maximum optical efficiency system. Importantly, this single quantity encapsulates all optical losses without the computational intensity of individually calculating the energy lost due to blocking and shading. In order to isolate the effects of geometric manipulations on the etendue of the system, perfect reflection and minimum optical error conditions are used. For two target apertures, a system that conserves etendue would require reflectors placed along a curve rather than a flat plane. Etendue conservation for a compact linear Fresnel can therefore be calculated as in Equation 2.

$$dU_0 = dU_1 + dU_2 \quad (2)$$

U_0 is defined as the etendue of the incoming radiation. At any given point along the curve, this incoming radiation can be split into two parts, U_1 and U_2 targeting aperture A1 and A2 respectively. The angle between the point along the curve M and the aperture A1 is defined as ϕ_1 , while the angle between point M and aperture A2 is defined as ϕ_2 as illustrated in Fig. 3. α is defined as the angle between the curve and the x axis

$$\cos \alpha = \cos(\phi_1 - \alpha) + \cos(\phi_2 + \alpha) \quad (3)$$

Equation 3 for etendue conservation (Chaves and Collares-Pereira, 2010) was used to determine a curve along which the mirrors are placed by varying the axis heights to maximise the collector surface area. This angle of the curve α must be derived for an infinitesimally small aperture width dl (see Fig.

5). Many curves meet this criteria, so the most compact curve was selected with the centre of the field along the reference plane of $y = 0\text{m}$ (Rungasamy et al., 2015). The receiver height from the reference plane to the focal point was chosen to be $H = 6\text{m}$, with a corresponding total field width of $D = 20.8\text{m}$. While the etendue conserving curve can be extended to multiple receivers, for this study a field with two receivers is used. The receivers are placed at $(0,6)$ and $(20.8,6)$.

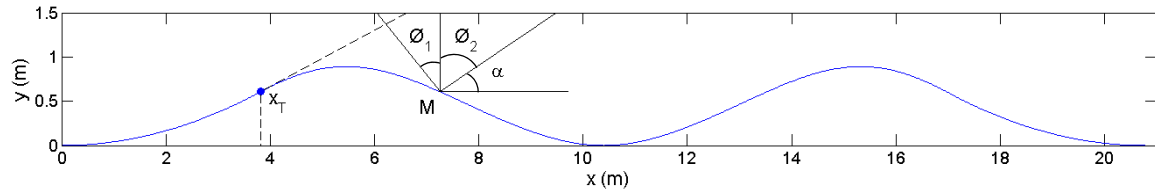


Fig. 3. Etendue-conserving curve for sun elevation angle of 0 degrees with $H = 6\text{m}$ and $D = 20.8$ (Rungasamy et al., 2015)

2. Method

2.1 Optics

Three collector fields were investigated; a flat CLFR field (flat-CLFR), an etendue-conserving CLFR field (ECCLFR) and the new concept, an off-peak etendue-conserving CLFR field (OP-ECCLFR). The flat CLFR field is a comparatively mature technology and as such will form the baseline for the comparison of the fields. The field was designed within Matlab, which then launched a script within the Monte Carlo ray tracing simulation software, SolTrace (Wendelin 2013). The desired number of ray intersections was set to 1 million and a Gaussian sun shape with a sigma of 3.1 was used with a $\text{DNI} = 1000 \text{ W/m}^2$ (an ideal summer day). The resultant ray data was written to a .csv file which was read back into Matlab for post processing. An example of a SolTrace simulation for the ECCLFR is shown in Fig.4. The yellow lines displayed are rays that hit the aperture.

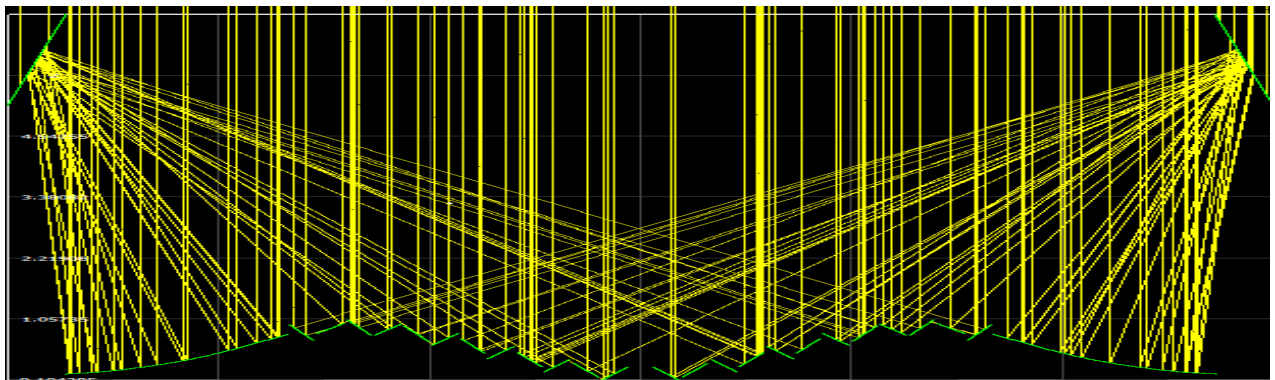


Fig. 4. SolTrace simulation of an etendue-conserving CLFR field $dl = 0.5 \text{ m}$, $r = 1$ and sun elevation angle of 0°

After the original curve that dictates the position of the mirror axes was found, the curve was discretized into discrete linear sections.

2.2 Generation of the curve

For etendue-conserving compact linear Fresnel fields, the curve itself must first be generated. Both the sun-tracking and off-peak ECCLFR fields have the same original curve; the distinction between the

fields occurs in the way that the mirrors track the sun for the non-vertical sun elevation angles experienced throughout the course of the day. The equation for etendue conservation was expressed as a residual function, R , which formed the objective function (see equation 4) to be minimised in Matlab using an unconstrained optimization function (`fminunc`). As the curve ought to approximate an infinitesimally small aperture, the domain needed to be divided into very small sections. A refinement study was performed in order to determine the number of divisions required to capture the curve accurately. A domain division of 100 000 (linear sections of 2.1×10^{-4} m) was able to capture the curve with errors of less than 0.1%. The unconstrained optimisation is performed for each division within the domain and the subsequent exit flag, gradient and hessian outputs of the function determine whether the optimisation is fully converged at a minimum.

From equation (3) we can derive the equation for the residual function

$$R = |\cos(\phi_1 - \alpha) + \cos(\phi_2 + \alpha) - \cos \alpha| \quad (4)$$

The resultant etendue-conserving curve is illustrated in Fig. 3. The point where the curve transitions from a single target section to a multi-target section was determined as the point at which the tangent to the curve passes through the opposite receiver. For this field the transition point was at $x = 3.8$ m, as indicated in Fig. 3.

2.3 Discretization of the curve

Two methods of discretization were investigated; a curve length-based discretization and a position-based discretization. These discretization methods can be applied to all the fields presented in this paper.

For the curve length-based discretization, the curve was approximated as a higher-order polynomial to calculate the total length and length of the single and multi-target sections, as it does not have an explicit function for the entire domain. In the case of the flat CLFR this was simply the length of a straight line in the x -direction.

The process of discretizing the domain required a specified mirror width and ratio between the mirrors targeting the two apertures. This domain was divided into the maximum number of mirrors of specified width that can be fit along it, creating a densely populated field, as illustrated in Fig. 5. The first section of the discretised curve is the single target section with mirrors targeting aperture A1, the middle section of the curve contains mirrors alternating between targeting apertures A1 and A2 in V formation and the final section of the discretised curve contains mirrors targeting aperture A2.

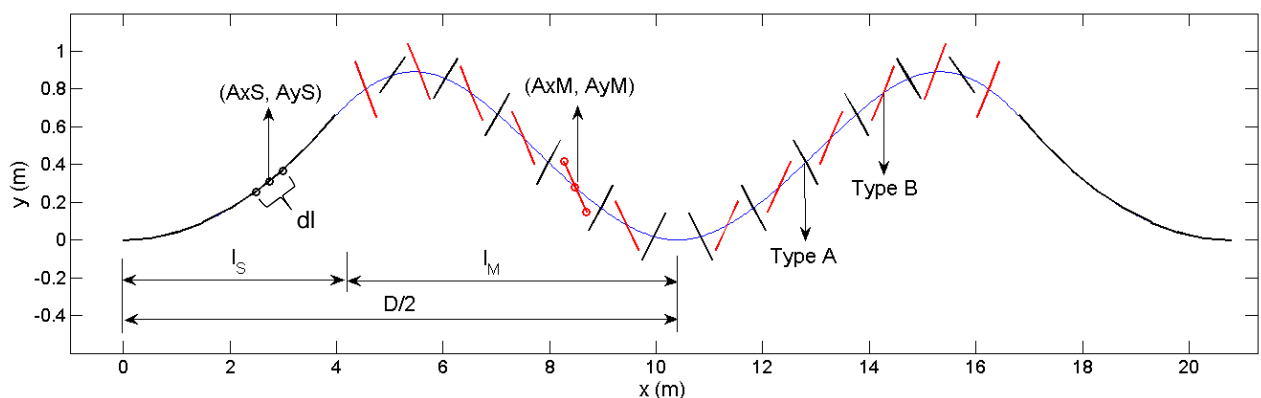


Fig. 5. Mirror field discretization process for a sun elevation angle of 0 degrees

The number of single-target mirrors (N_{mS}) was defined as the length of the single target curve (l_s) divided by the mirror width (dl)

$$N_{mS} = \text{round}\left(\frac{l_s}{dl}\right) \quad (5)$$

Within the multi-target section of the curve, there are two types of mirrors; Type A mirrors target the closest receiver for that section of the curve while Type B mirrors target the farther receiver for that section of the curve. These two types of mirrors are different widths, in order to maximise the amount of energy captured in the central section. In order to simplify that calculation, the two mirror widths (l_A and l_B) are expressed as a ratio (r). The width of the Type A mirrors (l_A) are set to the same width as the single target mirrors (dl) for simplicity

$$r = \frac{l_B}{l_A} = \frac{l_B}{dl} \quad (6)$$

Therefore the width of the Type B mirrors can be expressed in terms of the single target mirror width and ratio

$$l_B = r \cdot dl \quad (7)$$

and the combination of the two mirror widths can be expressed as follows

$$l_A + l_B = (1 + r) dl \quad (8)$$

The number of multi-target mirrors (N_{mM}) was defined as the length of the multi-target curve (l_m) divided by the mirror widths of both mirrors:

$$N_{mM} = \text{round}\left(\frac{l_m}{l_A + l_B}\right) = \text{round}\left(\frac{l_m}{(1 + r) dl}\right) \quad (9)$$

For the single-target section, the position of the axis in the x-dimension was

$$A_{xS} = \frac{dl}{2} + dl(i) \quad (10)$$

with i the index of the mirror. For the multi-target section, the position of the axis in the x-dimension was

$$\left. \begin{aligned} A_{xMlong} &= \frac{dl}{2} + dl(1+r)(i) \\ A_{xMshort} &= dl\left(1 + \frac{r}{2}\right) + dl(1+r)(i) \end{aligned} \right\} \text{ for } i = 0 : (n_M - 1) \quad (11)$$

A search function found the x value along the curve that was closest to the calculated value and the corresponding y value, then found the position of the axes in the y direction. For the flat CLFR, the y value for all axes was simply $y = 0$ m.

The discretization process originally proposed (Chaves and Collares-Pereira, 2010) suggested sizing based on the mirror's position within the field. This discretization process was investigated (Rungasamy et al., 2015) and compared to the process of selecting a mirror width and ratio. For the implementation in this paper, the incident radiation on the receiver aperture was measured at peak conditions as the etendue-conserving curve and discretization process were based on a vertical sun elevation angle.

Table 2

Comparison of the incident radiation for different discretization methods for a vertical sun elevation angle

Discretization method		Incident radiation on aperture [W]		Percentage loss from max power [%]		
Method	Equal	Aperture A1	Aperture A2	Aperture A1	Aperture A2	Avg % loss
Position based	Unequal	6273	6287	30.4	30.1	30.3
Position based	Equal	7482	7477	17.0	16.9	17.0
Curve length	Unequal	9015	9000	0	0	0
Curve length	Equal	8236	8199	8.6	8.9	8.8

The curve length-based discretization resulted in a higher incident radiation on the receiver aperture. Table 2 illustrates the comparison between the two methods of discretization. The total power of the plotted rays is the power per ray multiplied by the number of rays that hit the aperture A1 and A2 respectively. While the maximum radiation values were obtained when one allowed the mirrors to be sized individually, this creates significant challenges in the manufacturing of the mirrors. Therefore, Table 2 also includes a comparison to equal sections of mirror, which still resulted in higher incident radiation using the curve-length method of discretization.

As the curve length-discretization resulted in a higher incident radiation on the receiver aperture, it was used for this comparative study. However, as it requires a mirror width and ratio, the field was optimised for these parameters in order for the best possible field for each configuration to form the basis of the comparison.

2.4 Tracking the sun

The flat CLFR and sun-tracking ECCLFR simply rotate about a fixed axis throughout the course of the day to target aperture A1 and A2 as described in equation 12.

$$\beta(\theta) = \frac{\beta_0 + \theta}{2} \quad (12)$$

The original etendue-conserving mirror field was designed for vertical sun conditions and represented significant gains in optical efficiency of the collector under these conditions. During the day (considering an ideal summer day with a zenith and azimuth angle of 0°) however, etendue is not conserved as the mirrors simply rotate to track the sun. Therefore there is room for additional gains in the optical efficiency of the field if the principle of etendue conservation is applied throughout the day by modifying the equation for etendue conservation to include a non-vertical sun elevation angle relative to the vertical (θ).

For the off-peak ECCLFR, the modified equation for off-peak etendue conservation was derived as

$$\cos(\alpha - \theta) = \cos(\phi_1 - \alpha) + \cos(\phi_2 + \alpha) \quad (13)$$

This was once again expressed as a residual objective to be minimized in a Matlab unconstrained optimization

$$R_{\text{offpeak}} = |\cos(\phi_1 - \alpha) + \cos(\phi_2 + \alpha) - \cos(\alpha - \theta)| \quad (14)$$

Fig. 6 illustrates the curves generated for different sun elevation angles ranging between 0° and 40° . The central dip in the 0° curve lifts up for other sun elevation angles in order to prevent increased shading by the peak of the curve closest to the incoming sun. The entire curve lifts and shifts in the direction opposite to that of the incoming sun, such that even the mirrors in the furthest single target section are still hit by the sun. The maximum elevation change will occur for the mirrors in the centre of the field, where they will be lifted 1.7m over the course of the day. Subsequent sections of this paper will investigate the economic feasibility of this field, given that this would require extra drives for this vertical actuation and therefore significant extra costs are introduced. This action also creates a larger parabolic single target section for those mirrors closest to the incoming sun.

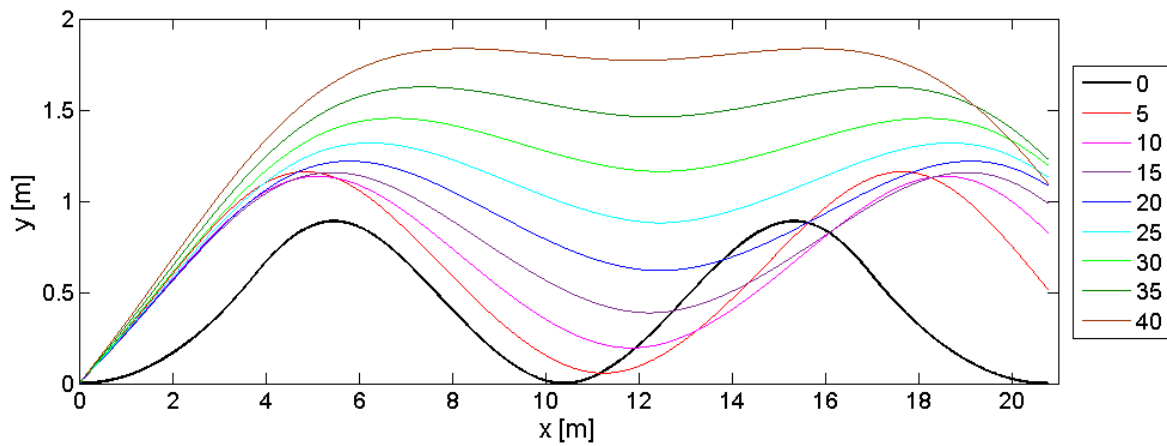


Fig. 6. Off-peak Etendue-conserving curves along the x domain for different sun elevation angles in 5° increments

This trend continues up to a maximum incoming sun elevation angle of 40° , at which point the single target section of the collector furthest from the sun becomes exponentially higher to prevent shading. This phenomenon for sun elevation angles larger than 40° is illustrated in Fig. 7.

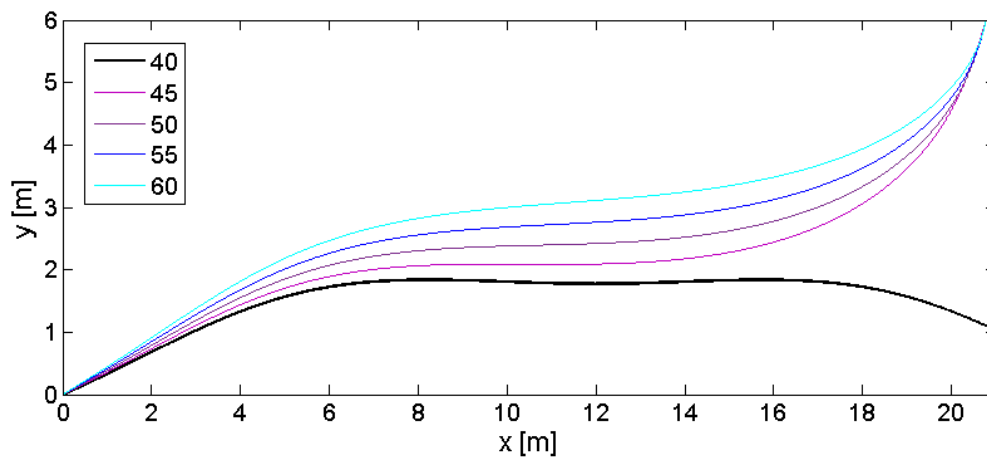


Fig. 7. Off-peak etendue-conserving curve along the x domain for sun elevation angles greater than 40° in 5° increments

Mirror setups following the curves in Fig. 7 are impractical to implement, so for higher sun elevation angles the etendue-conserving curve at 40° is used as the limit of the optimization and the mirrors subsequently track the sun as normal with their centres remaining along the 40° curve.

For the off-peak ECCLFR plant the mirrors' axis points lift up to match the off-peak etendue-conserving curve and the mirrors also rotate to track the sun throughout the course of the day. While the equation for targeting the aperture (equation 12) remains the same, it must be noted that due to the different position of the mirror axis both the original angle (β_0) and the incoming sun elevation angle (θ) will change throughout the day, resulting in the mirror having a different targeting angle to the corresponding mirror of the sun-tracking ECCLFR model.

2.5 Design investigation

A design investigation was necessary due to the integer-based nature of the number of mirrors. The curve-based discretization allowed for the number of mirrors to vary freely, creating a response surface that is neither continuous nor differentiable. Conventional gradient-based optimization methods can therefore not be used. Instead, an iterative process of response-surface construction and domain-reduction strategies are used for each collector configuration and the design points are connected up linearly. In order to create a design exploration that is independent of the optics of the receiver chosen, the same simple aperture is used for each case to measure the reflected radiation of the field. The aperture is at an angle of 30° from the horizontal and is therefore directed at the centre of the mirror field. The fields were generated within Matlab and a SolTrace script was run for a specified sun elevation angle. In order to evaluate optical performance more thoroughly, SolTrace simulations were run throughout an ideal summer's day, at 5° intervals. The ray data are processed for both apertures at each sun angle and the daily performance is evaluated based on how much of the incident radiation on the collector aperture is reflected onto the receiver aperture throughout the day.

Initially, 45 design points were used with mirror widths between 0.1-1.6m (0.1, 0.3, 0.5, 0.7, 0.8, 0.9, 1.1, 1.3 and 1.5) and for mirror ratios between 0.05-2 (0.05, 0.5, 1, 1.5 and 2). The design points were chosen to give a wide selection of commonly available mirror widths. The mirror ratio determined the width of the mirror targeting the furthest receiver in the central section relative to the width of the mirror targeting the closest receiver. As two parameters were investigated within this section, the increments of change were varied slightly based on which sections of the response surface had the most rapid changes in gradient. The mirror field was simulated for sun elevation angles from -65° to 65° in 5° intervals. The resultant incident radiation was stored and the integer values are presented within this optimization. A single response surface was constructed for full-day performance for an ideal summer day (sun in a plane directly overhead). Then, based on the information obtained, a successive response surface was created.

The field configurations were then compared on the basis of optical efficiency and cost. The transition point between single and multi-target sections was the same as the point used in the design of the etendue-conserving field in order to compare the two fields as directly as possible. The height of the receiver was set at $H = 6\text{m}$ and width of the field is calculated as $D = 2H \tan 60^\circ$ (in this case $D = 20.8\text{m}$).

3. Results

3.1 Case I: Flat Compact Linear Fresnel (Flat CLFR)

Fig. 8 shows the response surface of the total incident radiation throughout the day versus mirror width and ratio for the Flat CLFR case.

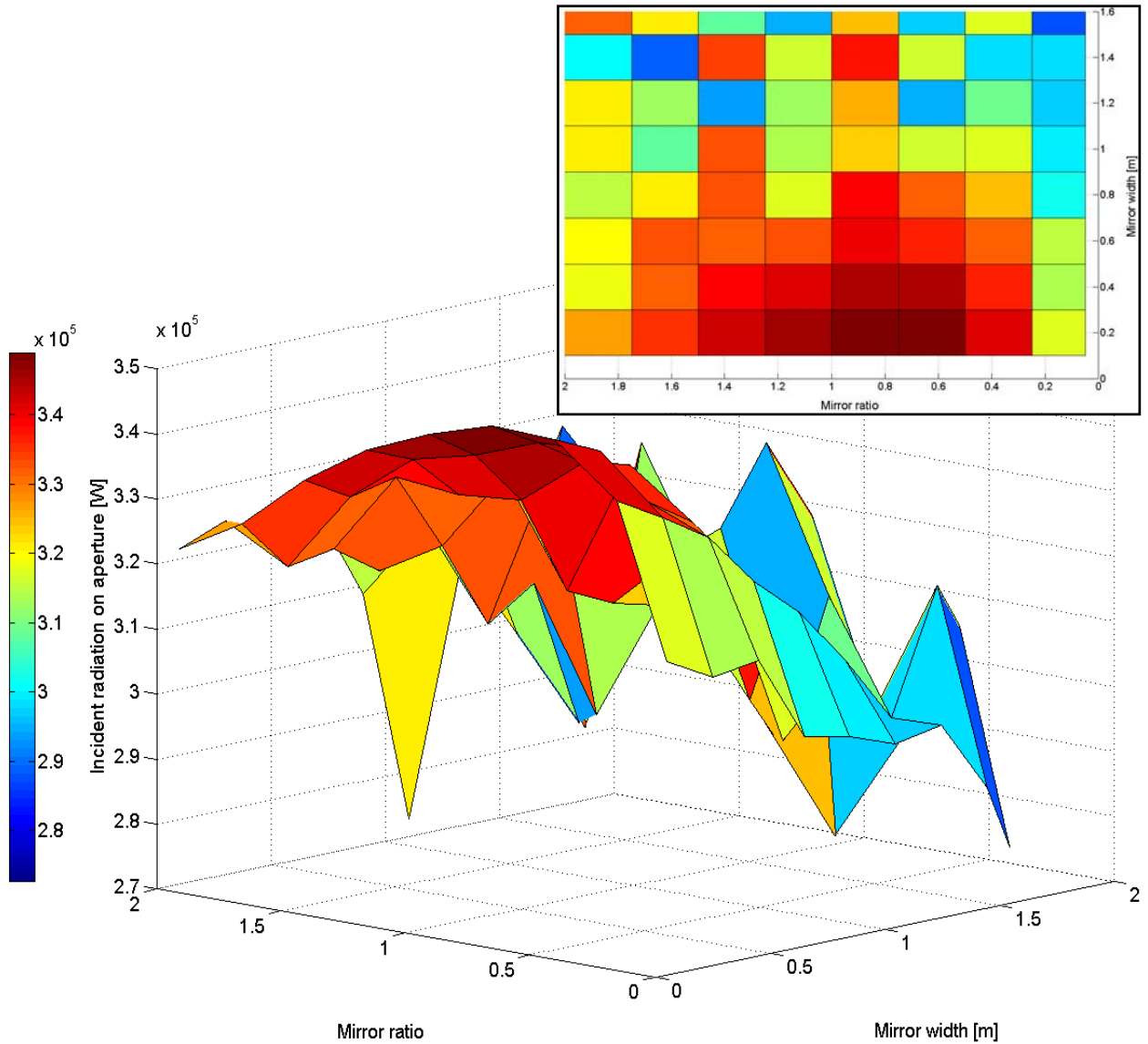


Fig. 8. Response surface of the total incident radiation throughout the day versus mirror width, (dl [m]) and ratio for a flat CLFR model

The response surface is extremely jagged and discontinuous, making it difficult to identify a clear trend especially for the larger mirror widths. This is due to the curve length algorithm populating the curve as densely as possible, combined with the integral nature of the number of mirrors. For wider mirrors, a reduction in the number of mirrors could introduce significant gaps in the field, thus causing a decrease in the amount of incident radiation the collector field is able to capture. The total incident radiation for shorter mirror widths is generally higher than for long mirror widths and a parabolic shape is formed for the mirror ratios, with peaks lying between 0.5 and 1.

Fig. 9 illustrates the performance of different mirror configurations throughout the day. It is important to note that the form of the incident radiation curves adheres very strongly to the form of the available energy curve throughout the day. A flat CLFR field therefore captured a relatively consistent portion of the available energy for any given sun elevation angle.

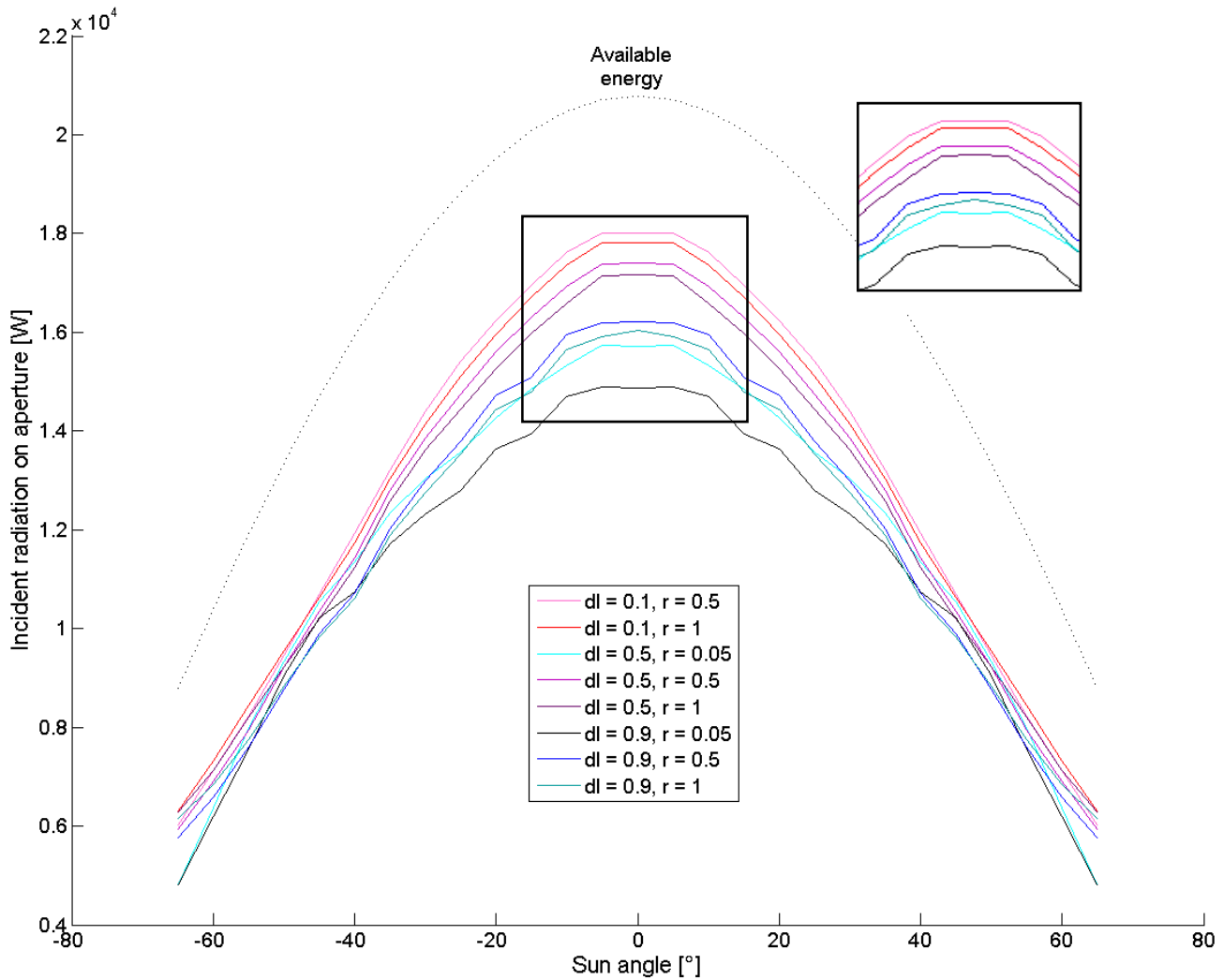


Fig. 9. Incident radiation versus sun elevation angle for different mirror widths [m] and ratios for flat-CLFR

3.2 Case II: Sun-tracking Etendue Conserving Compact Linear Fresnel (ECCLFR)

The above design investigation was next performed for a variety of mirror widths and ratios to construct a response surface for the ECCLFR design.

The trend of the response surface in Fig. 10 tends towards higher levels of reflected radiation on the apertures for mirror ratios of 1, with a smoother trend evident for short mirror widths. This smoothing effect at short mirror widths is due to the fact that changes in the mirror width or ratio also cause changes to the number of mirrors. For smaller mirrors this resulted in smaller changes to the surface area of the collector field as the number of mirrors vary. The lowest incident radiation is associated with the lowest mirror ratio of 0.05. This is likely due to the fact that the resultant mirrors at this ratio are so short that they do not effectively capture the rays that are reflected through the highest angles. The combination of a small mirror and high reflection angle results in a very small contribution from these mirrors. Moreover small mirror ratios can introduce large gaps in the central section, resulting in larger losses for vertical or almost vertical sun elevation angles.

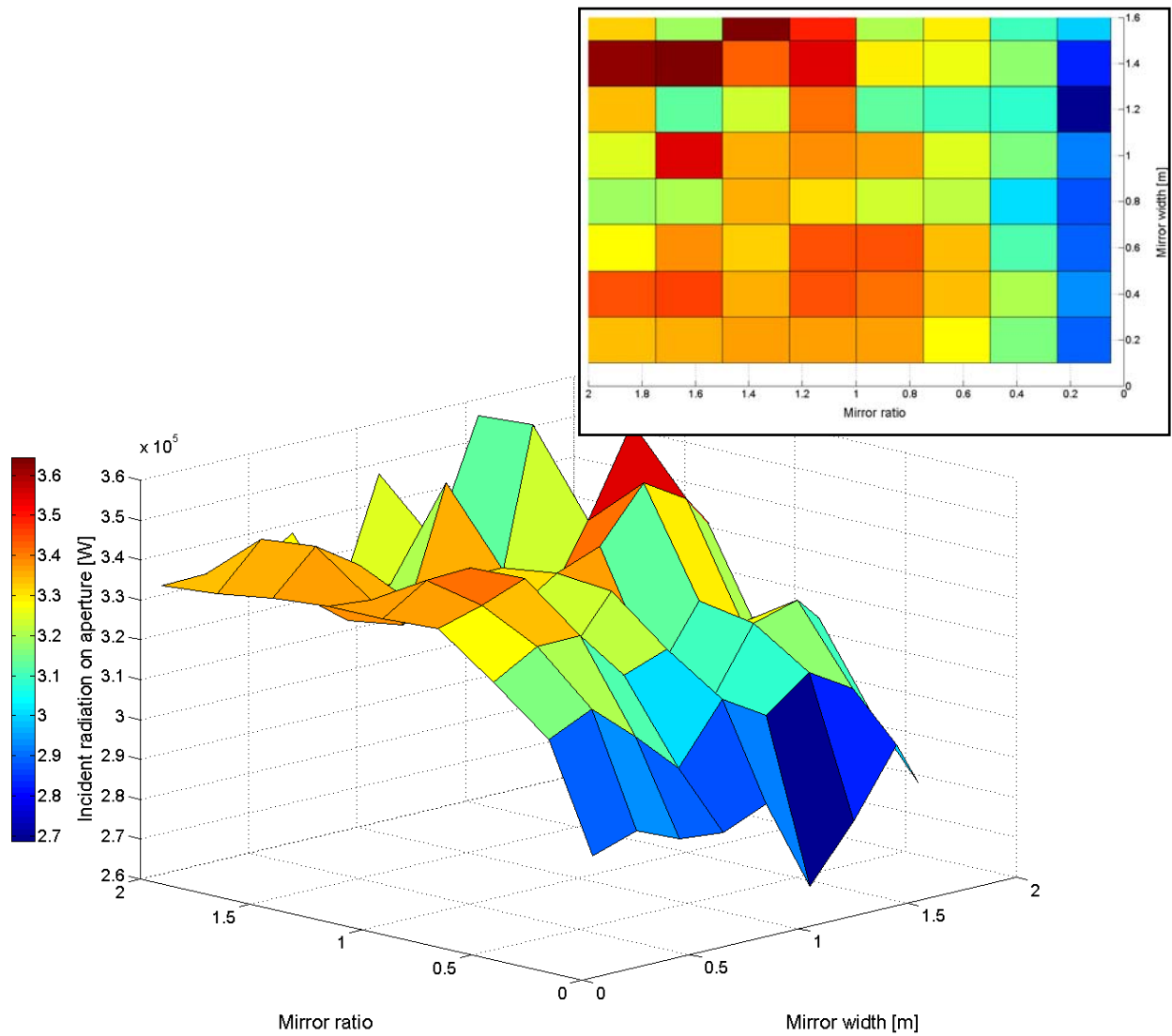


Fig. 10. Response surface of total reflected radiation on the aperture versus mirror width and ratio for a sun-tracking ECCLFR field

In order to fully understand the resultant total reflected radiation on the aperture it is valuable to examine the mirror field performance throughout the course of the day, as shown in Fig. 11.

Fig. 11 shows that the ratio of 0.05 performs especially poorly at peak conditions. For all other ratios, the major distinction in performance occurs at the vertical sun elevation angle as the curves converge to very similar levels of incident radiation at higher sun elevation angles.

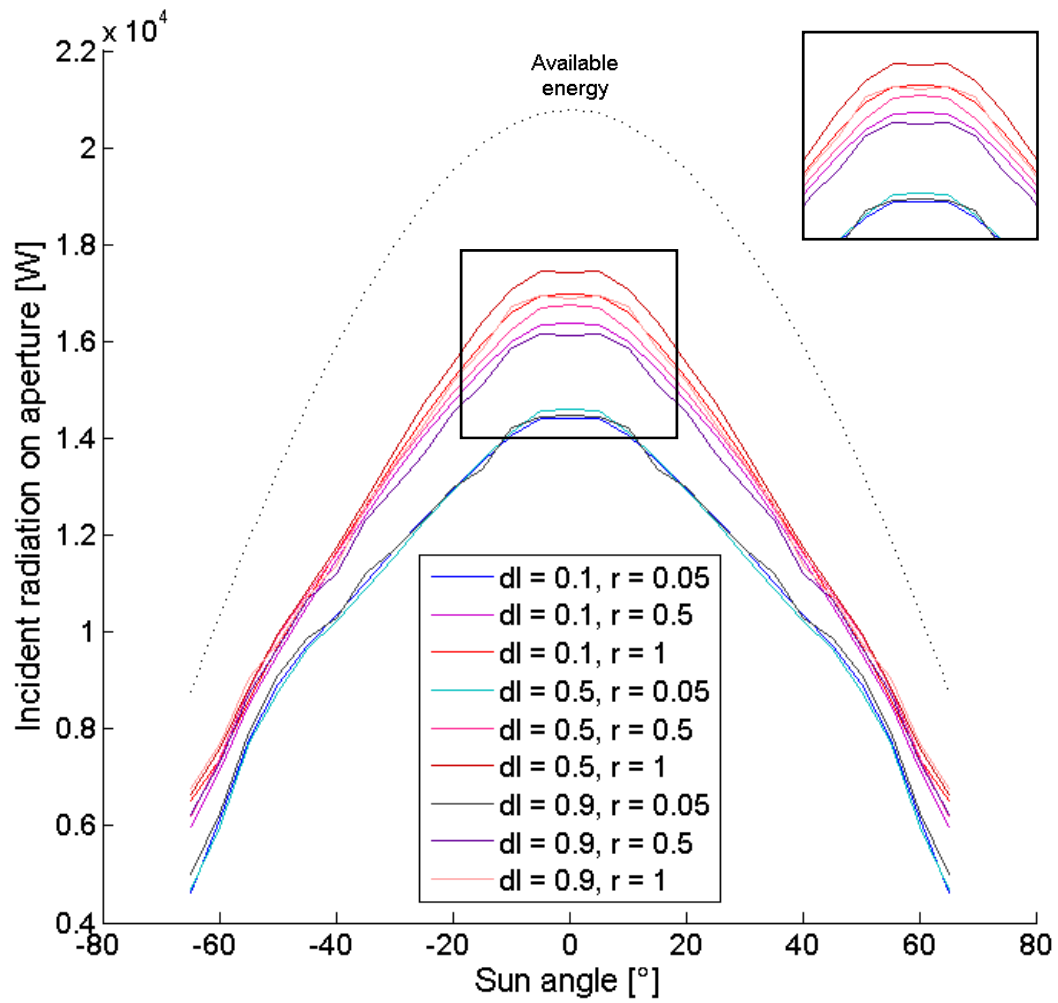


Fig. 11. Incident radiation versus sun elevation angle for different mirror widths [m] and ratios for sun-tracking ECCLFR

3.3 Case III: Off-peak Etendue Conserving Compact Linear Fresnel (O-P ECCLFR)

Constructing a response surface with a mirror field adhering to equation 13 results in the surface plotted in Fig. 12.

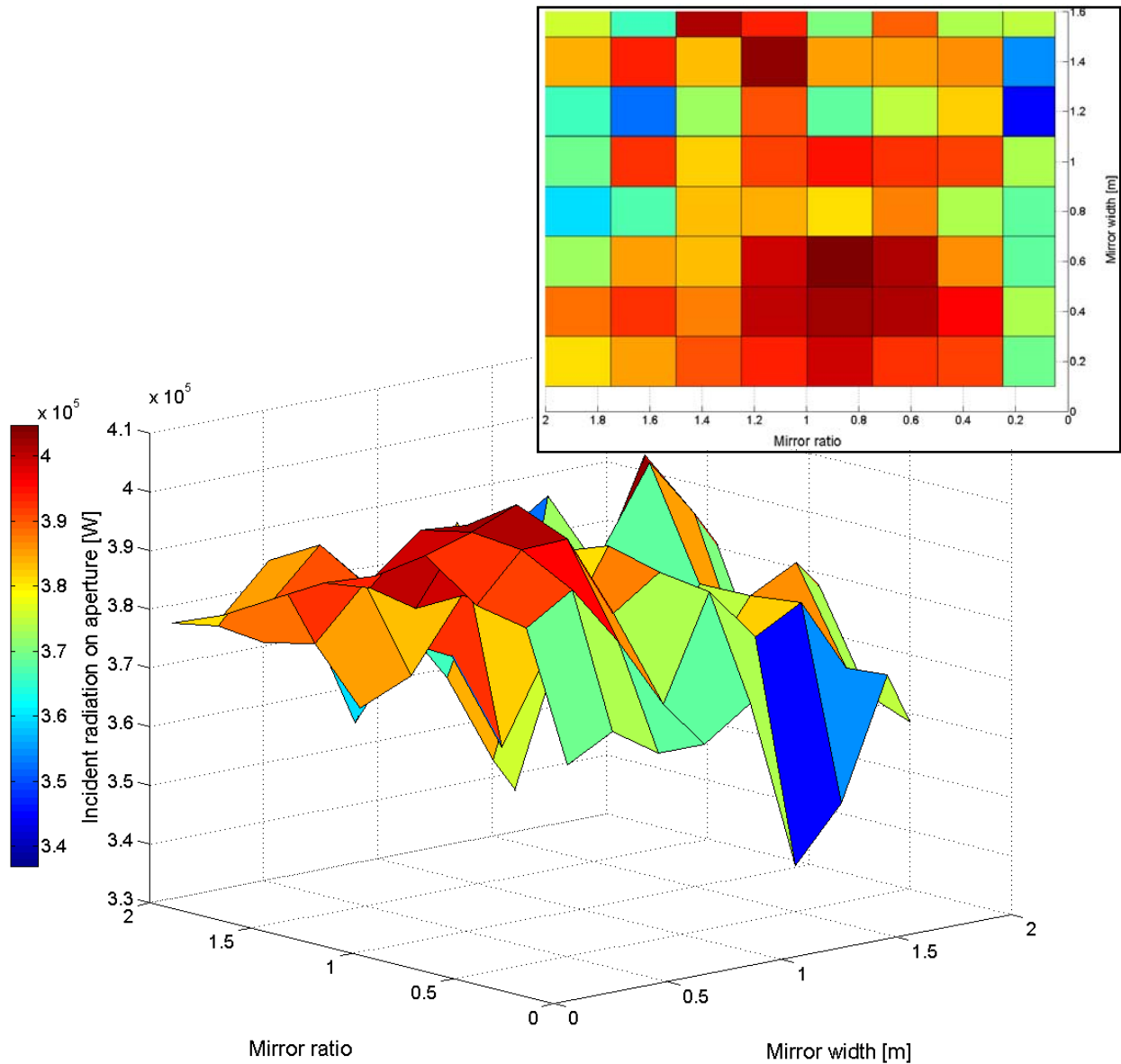


Fig. 12. Response surface of total incident radiation versus mirror width and ratio for an off-peak ECCLFR field

The highest incident radiation in Fig. 12 typically occurred at ratios between 0.5-1 but there were several mirror widths that produced similarly high amounts of reflected radiation. The general trend was towards a higher incident radiation on the aperture for shorter mirror widths. A mirror width of 1.3 m seems to be notable exception as an outlier maximum at a relatively large mirror width.

Fig. 13 shows that the peak incident radiation is the same for both sun-tracking and off-peak ECCLFR as it is the same field. It is for non-vertical angles that the curves significantly change form, with the off-peak curves capturing the maximum available energy for sun elevation angles above 45° . This occurs even for fields with poor peak performance, such as for ratios of 0.05.

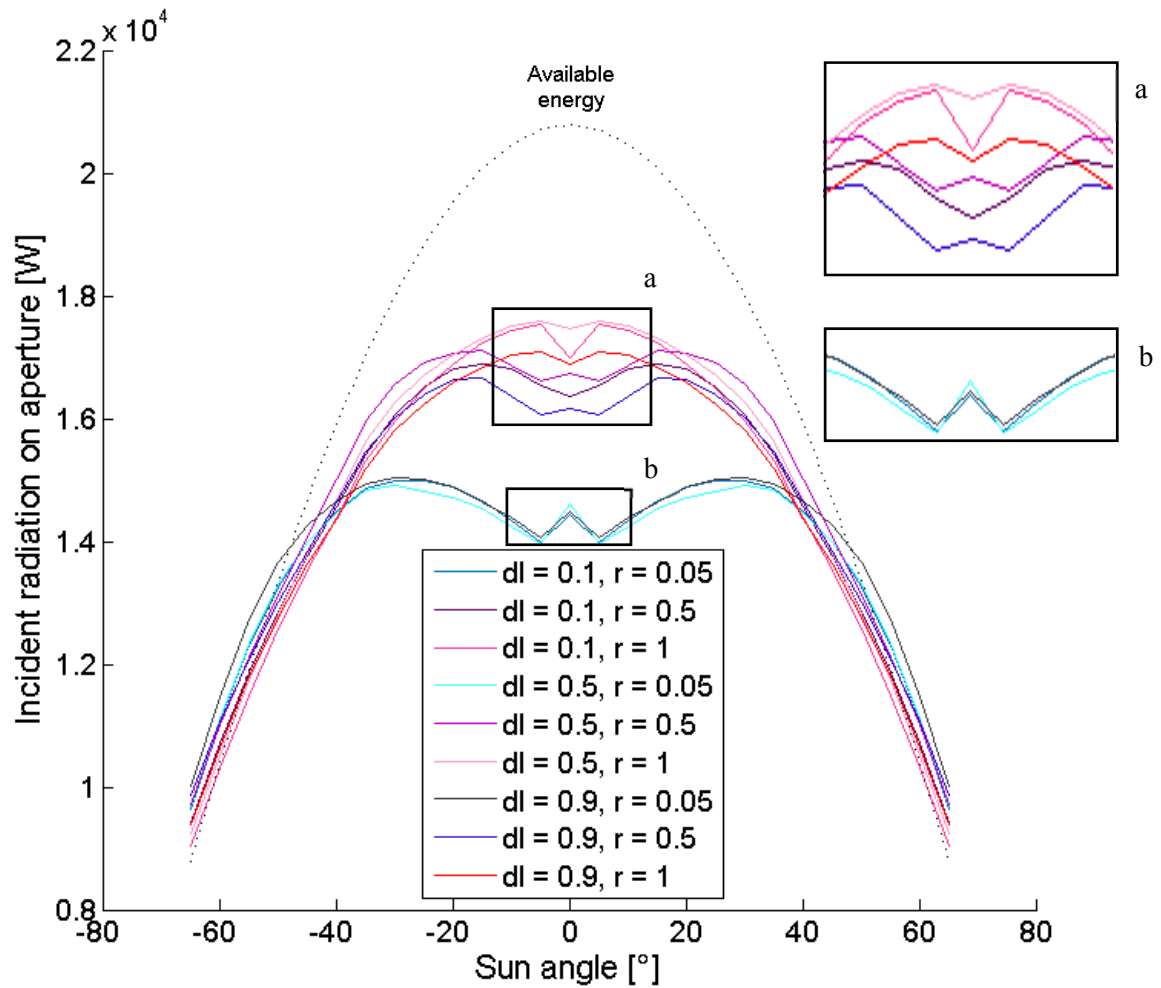


Fig. 13. Incident radiation versus sun elevation angle for different mirror widths [m] and ratios for an off-peak ECCLFR field

3.4 Comparison of Field Optics

In order to better understand the differences in the three fields, Fig. 14 illustrates the levels of incident radiation for the three designs using the same mirror width and ratio.

Fig. 14 shows that the increases in efficiency difference between the flat and sun-tracking ECCLFR occur around the peak incident radiation levels, while the descent of the curve is relatively similar. The difference between the off-peak ECCLFR field and the other two fields is that it not only increases the incident radiation levels around the peak, but also significantly increases levels of radiation in the descent of the curve at higher sun elevation angles.

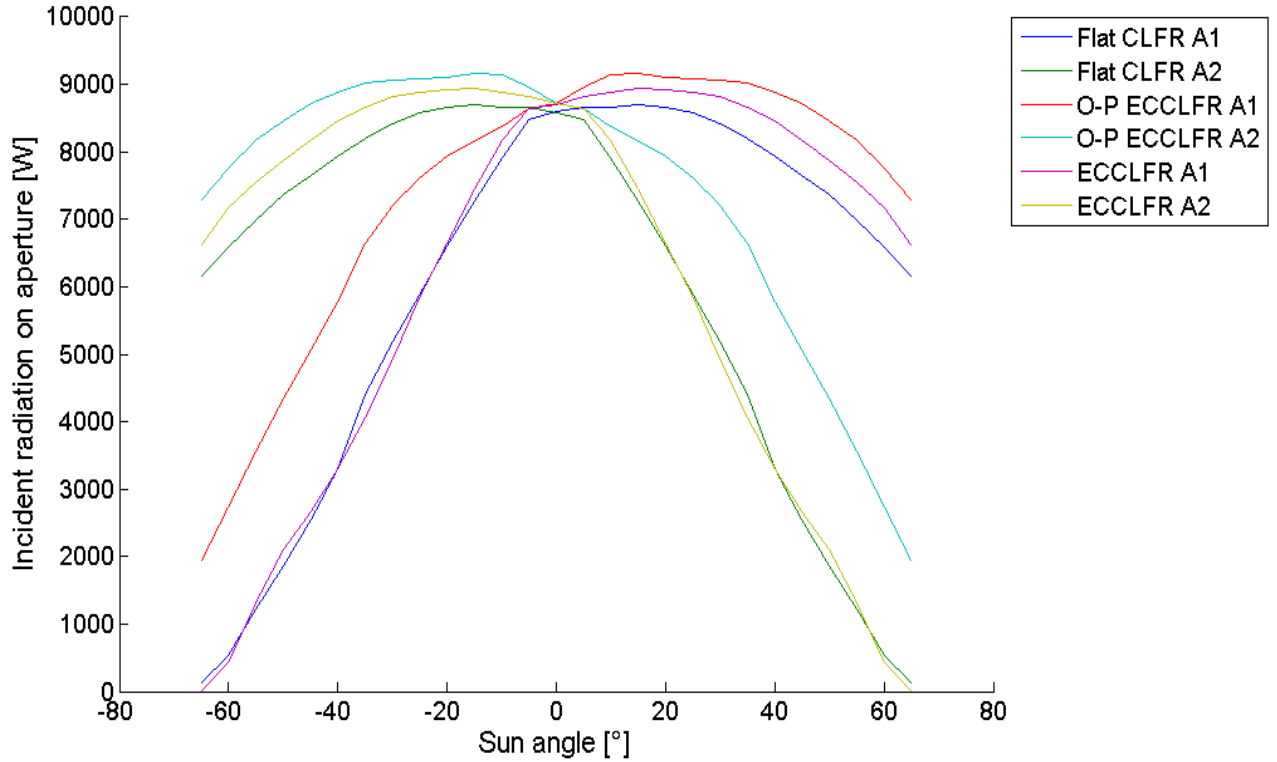


Fig. 14. Incident radiation on each receiver aperture (A1 and A2) versus sun elevation angle for flat, sun-tracking etendue conserving and off-peak etendue conserving CLFR fields

For all mirror configurations, the off-peak ECCLFR significantly outperformed both the flat CLFR and the sun tracking ECCLFR. This is specifically due to its performance for off-peak (higher) sun elevation angles, as it is identical to the sun-tracking model for a vertical sun elevation angle. In a similar trend to the sun-tracking ECCLFR, the starkest gains were found for wider mirrors and a ratio around 1 (implying that the mirrors aimed at the opposing receivers in the central section are the same width). The maximum disparities occur at $dl = 1.3$ m, $r = 1.5$ and $dl = 1.6$ m, $r = 1$. This is largely due to the flat CLFR performing more poorly for larger mirror widths as opposed to the ECCLFR performing particularly well, however it does mean that the design allows for more flexibility in that wider mirrors can achieve similarly high incident radiation levels.

The degree to which the off-peak etendue-conserving curve reduced optical losses becomes more pronounced at higher sun elevation angles where shading losses in particular would be most prevalent. The receiver farthest from the incoming sun receives significantly less incident radiation than the closer receiver as the sun elevation angle increases. In practice this could cause large heat disparities between the two receivers which may lead to additional thermal design challenges for the plant. While this disparity does occur to a certain degree in either model, the off-peak etendue-conserving field significantly reduced the disparity of incident radiation on the two receivers, thereby going some way to mitigating these thermal design challenges.

The mean geometric intercept factor (Equation 15) of the collector field is defined as the proportion of the total radiation that hits the field (defined in Equation 16) that is reflected from the collector onto the receiver aperture (Bendt et al, 1979). The receiver aperture is constant at 2m and the collector field is optimised as specified above.

$$\gamma = \frac{\dot{Q}_{T,aperture}}{\dot{Q}_{T,field}} \quad (15)$$

$$\dot{Q}_{field} = D_{field} \cdot DNI \cos \theta \quad (16)$$

Table 3-5 present the geometric intercept factors for all mirror widths and ratios for the flat CLFR, ECCLFR and O-P ECCLFR, respectively.

Table 3: Flat CLFR geometric intercept factor

		Mirror ratio								
		0.05	0.25	0.5	0.75	1	1.25	1.5	1.75	2
Mirror width [m]	0.1	0.721	0.774	0.792	0.793	0.786	0.777	0.762	0.743	0.731
	0.3	0.712	0.765	0.784	0.783	0.775	0.770	0.753	0.725	0.737
	0.5	0.715	0.755	0.763	0.773	0.756	0.754	0.757	0.728	0.726
	0.7	0.685	0.736	0.753	0.769	0.721	0.757	0.729	0.717	0.733
	0.8	0.696	0.738	0.738	0.739	0.730	0.712	0.752	0.681	0.710
	0.9	0.681	0.722	0.719	0.734	0.713	0.757	0.698	0.729	0.701
	1.1	0.675	0.702	0.670	0.740	0.709	0.667	0.709	0.730	0.620
	1.3	0.679	0.678	0.717	0.767	0.718	0.759	0.657	0.684	0.712
	1.5	0.654	0.721	0.674	0.738	0.670	0.700	0.730	0.754	0.697
	1.6	0.631	0.705	0.660	0.625	0.656	0.688	0.714	0.647	0.684

Table 4: Sun tracking ECCLFR geometric intercept factor

		Mirror ratio								
		0.05	0.25	0.5	0.75	1	1.25	1.5	1.75	2
Mirror width [m]	0.1	0.657	0.718	0.743	0.766	0.765	0.765	0.762	0.757	0.755
	0.3	0.666	0.729	0.758	0.774	0.781	0.763	0.786	0.782	0.755
	0.5	0.655	0.708	0.758	0.783	0.782	0.754	0.769	0.744	0.750
	0.7	0.653	0.684	0.730	0.734	0.751	0.762	0.729	0.724	0.767
	0.8	0.680	0.701	0.735	0.776	0.793	0.774	0.770	0.813	0.728
	0.9	0.663	0.717	0.739	0.764	0.767	0.763	0.804	0.739	0.719
	1.1	0.610	0.702	0.702	0.709	0.777	0.736	0.711	0.758	0.789
	1.3	0.642	0.721	0.742	0.747	0.807	0.779	0.826	0.823	0.716
	1.5	0.679	0.705	0.749	0.729	0.792	0.828	0.724	0.754	0.689
	1.6	0.655	0.686	0.735	0.714	0.775	0.679	0.709	0.740	0.674

Table 5: Off-peak ECCLFR geometric intercept factor

		Mirror ratio								
		0.05	0.25	0.5	0.75	1	1.25	1.5	1.75	2
Mirror width [m]	0.1	0.839	0.888	0.892	0.907	0.894	0.886	0.875	0.864	0.856
	0.3	0.849	0.900	0.910	0.912	0.908	0.881	0.893	0.882	0.851
	0.5	0.837	0.876	0.911	0.920	0.907	0.870	0.875	0.846	0.842
	0.7	0.837	0.849	0.879	0.866	0.873	0.871	0.835	0.818	0.847
	0.8	0.862	0.862	0.879	0.909	0.909	0.883	0.864	0.888	0.825
	0.9	0.849	0.889	0.891	0.897	0.890	0.868	0.891	0.840	0.804
	1.1	0.783	0.868	0.851	0.835	0.887	0.846	0.801	0.831	0.839
	1.3	0.804	0.878	0.875	0.875	0.917	0.871	0.895	0.873	0.814
	1.5	0.850	0.849	0.885	0.841	0.894	0.912	0.831	0.852	0.779
	1.6	0.830	0.837	0.874	0.832	0.880	0.796	0.818	0.833	0.765

The mean geometric intercept factor for the off-peak ECCLFR is $\gamma = 0.863$, while the maximum geometric intercept factor obtained was $\gamma = 0.92$. Several configurations achieve intercept factors of over 0.90. The sun-tracking ECCLFR in comparison has a mean geometric intercept factor of $\gamma = 0.739$ and a maximum of $\gamma = 0.828$ while the flat CLFR has a mean geometric intercept factor of $\gamma = 0.721$ and a maximum of $\gamma = 0.793$.

The average percentage gain when comparing the off-peak etendue-conserving model to the flat CLFR model is 20% based on the geometric intercept factor. The sun-tracking ECCLFR model is 2% more efficient on average when compared to the flat CLFR. This represents a significant gain in efficiency for the OP-ECCLFR and was largely due to the off-peak performance of the field, which was significantly better than both the flat and etendue-conserving sun-tracking fields.

Fig. 15 confirmed that the major advantage of the off-peak ECCLFR field was at higher sun elevation angles as the incident radiation decreases at a much slower rate. In the optimum field, the ECCLFR slightly outperformed the O-P ECCLFR at sun elevation angles of 0-20°.

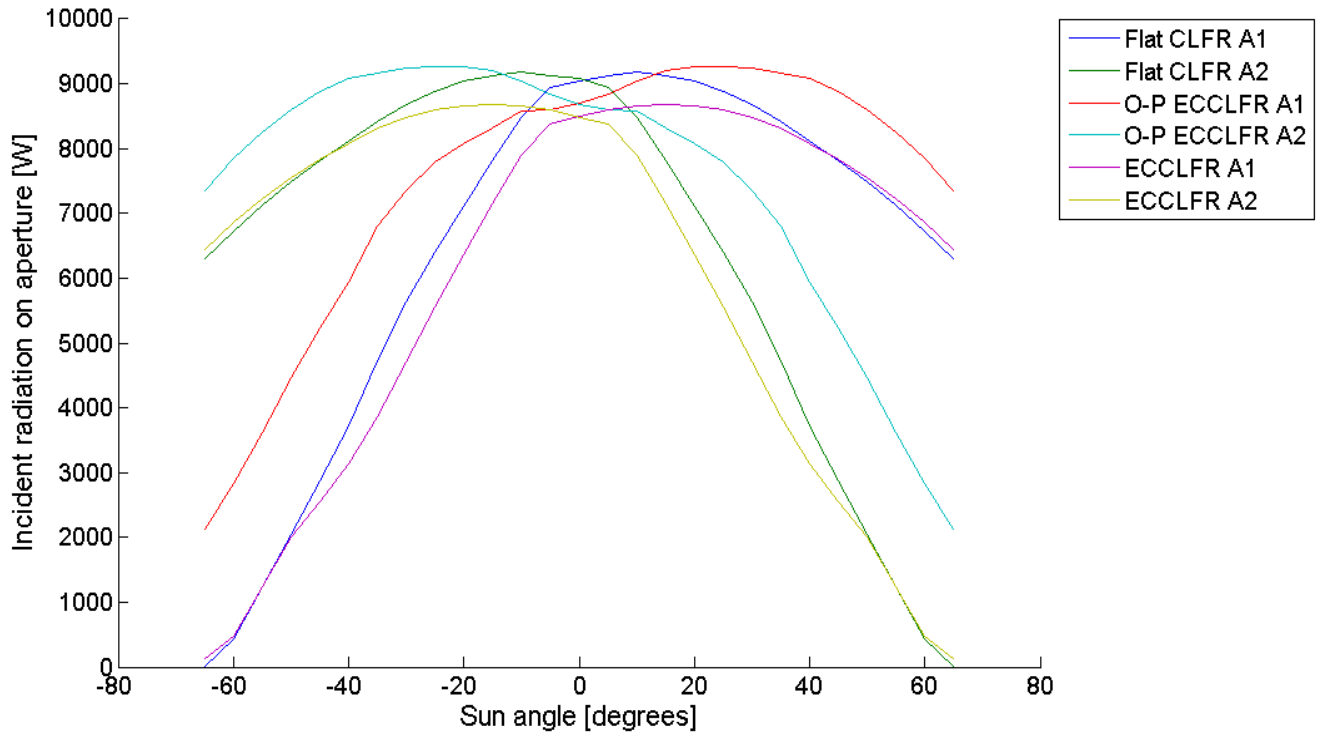


Fig. 15. Incident radiation on each receiver aperture (A1 and A2) versus sun elevation angle for the best configuration of flat, sun-tracking etendue-conserving and off-peak etendue-conserving CLFR fields

Using Bendt et al's (1979) definition for nominal optical efficiency and the following material properties: the mirror solar reflectivity $\rho = 0.92$, the glass transmissivity $\tau = 0.95$ and the absorber tube absorptivity $\alpha = 0.94$, the optical efficiency for the three models is calculated as in Equation 17:

$$\eta_{opt} = \gamma\rho\tau\alpha = \gamma \cdot (0.92) \cdot (0.95) \cdot (0.94) = 0.82 \cdot \gamma \quad (17)$$

The resultant mean nominal optical efficiency for the off-peak ECCLFR is $\eta_{opt0} = 0.71$ with a maximum optical efficiency of $\eta_{opt0} = 0.76$. The sun-tracking ECCLFR has a mean optical efficiency of $\eta_{opt0} = 0.61$ with a maximum of $\eta_{opt0} = 0.68$, while the flat CLFR has a mean optical efficiency of $\eta_{opt0} = 0.6$ with a maximum of $\eta_{opt0} = 0.65$.

3.5 Comparison of Field Costs

While the off-peak ECCLFR is significantly more optically efficient, the more complex design would likely cost more due to the requirement of both vertical movement and rotation. The etendue-conserving CLFR field has costs in the form of additional support structure to place mirrors at different heights to form a curve, while the off-peak etendue conserving CLFR has costs in the form of both the additional support structure and an additional drive for the vertical actuation of the mirrors. This could represent a significant increase in the costs of the collector field. The overall metric used to determine whether this efficiency gain would be worthwhile is whether electricity could be produced cheaper than the levelized cost of electricity (LEC) for a standard linear Fresnel plant with the same increase in optical efficiency due to the collector modifications made for the sun-tracking ECCLFR and the off-peak ECCLFR.

Despite exact costing values being difficult to obtain, some LFR economic models are available. The most detailed of these is a costing model by Mertins (2009), which breaks the solar field costs down into a primary mirror coefficient (C_m), a cost for the receiver structure (C_H), the gaps between the mirrors (C_d) and the receiver costs (C_{rc}), as described in Table 6. While this breakdown is well detailed, it is specific to the Solarmundo single LFR system with mirror widths of 0.5m and gaps of 0.01m. The coefficients were generalized by making the assumption that the variation for gap and mirror dependent coefficients is linear (Moghimi et al., 2017; Ardekani, 2017).

Table 6: Cost coefficients and specifications (Mertins et al., 2009; Moghimi et al., 2017; Ardekani, 2017) for a 50MW plant

Coefficient	Cost	Specifications
C_m	30.5 € / m ²	Primary mirror costs including structure, mounting and elevation and the driving motors and controllers, etc. for N_{pr} number of mirrors
C_H	19.8 € / m ²	Costs for the receiver height $H = 9$ m and mirrors mounted 4m off the ground
C_d	11.5 € / m ²	Costs of the primary mirror gaps
C_{rc}	654 € / m	Specific costs of the receiver for an aperture $D_a = 0.219m$
λ_I	640 000 €	Cost of infrastructure
λ_{PU}	33 600 000 €	Cost of power plant unit
λ_0	4 002 000 €	Piping and steam traps
κ_e	0.225	Project efforts (percentage of total investment that includes engineering, project management, contractor and licensor rights)
κ_a	0.09368	Annuity factors as a fraction of total investment for a duration of 25 years with an interest rate of 8%
κ_i	0.01	Annual insurance cost as a fraction of total investment
$\kappa_{O\&M}$	0.02	Annual operation and maintenance cost as a fraction of total investment
κ_u	0.05	Uncertainties as a fraction of total investment

The direct specific collector cost (C_c^d) is calculated as in Equation 18:

$$C_c^d = \frac{C_m N_m + C_H (4 + H) + C_d (N_{pr} - 1)G + C_{rc}}{N_m \cdot dl} \quad (18)$$

The total cost of the plant (λ_{total}) is then

$$\lambda_{total} = \left[(C_c^d \cdot A_c + \lambda_0) \cdot (1 + \kappa_e) + C_l \cdot A_c \cdot \left(1 + \frac{G}{dl} \right) + \lambda_I \right] \cdot (1 + \kappa_u) + \lambda_{PU} \quad (19)$$

The levelized cost of electricity is calculated based on the annual cost of the plant (λ_a) and the annual electricity yield (E_{el})

$$\lambda_a = (\kappa_a + \kappa_i + \kappa_{O\&M}) \cdot \lambda_{total} \quad (20)$$

$$LEC = \frac{\lambda_a}{\int_{year} E_{el} dt} \quad (21)$$

Therefore if one uses a constant levelized cost of electricity of $LEC = 0.167 \text{ €/kWh}$ and the annual costs as an independent variable, the required nominal optical efficiency can be calculated by finding the corresponding annual electrical yield.

$$\int_{year} E_{el} dt = \frac{\lambda_a}{LEC} \quad (22)$$

The annual electrical yield is dependent on the optical, thermal and power block efficiency's as well as the amount of incoming radiation

$$\int_{year} E_{el} dt = \eta_{opt} \cdot \eta_{th} \cdot \eta_{pb} \cdot \dot{q}_{in} \quad (23)$$

The optical efficiency can be made the subject of this formula in order to calculate the required nominal optical efficiency for a given total plant cost

$$\eta_{opt} = \frac{\int_{year} E_{el} dt}{\eta_{th} \cdot \eta_{pb} \cdot \dot{q}_{in}} \quad (24)$$

As an example, Häberle et al. (2002) report a thermal efficiency of 0.607 and a power block efficiency of 0.33.

The annual optical efficiency is defined by Mertins et al (2009) to be the product of the nominal optical efficiency (η_{0opt}), the shading efficiency (η_{sh}) and the effects of the Incidence Angle Modifier ($\kappa_{\tau\alpha}$):

$$\eta_{opt} = \eta_{0opt} \cdot \eta_{sh} \cdot \kappa_{\tau\alpha} \quad (25)$$

$$\eta_{0opt} = \frac{\eta_{opt}}{\eta_{sh} \cdot \kappa_{\tau\alpha}} \quad (26)$$

This process uses the optical efficiency at vertical sun elevation angle, the shading efficiency and the Incidence Angle Modifier in the transversal direction to predict optical efficiency throughout the day. However, the offpeak ECCLFR and suntracking ECCLFR fields have the same peak efficiency but very different efficiencies throughout the course of the day. Therefore using this equation as is will simplify out that efficiency gain. As the performance of the field is evaluated using SolTrace simulations throughout the course in 5° increments this can form the basis of an integral value of optical efficiency throughout the course of the day, representing the product of the nominal optical efficiency and shading efficiency.

The Incidence Angle Modifier can be factorized into factors in the longitudinal and transversal planes (McIntire, 1982; Hertel et al, 2015)

$$\kappa_{\tau\alpha} = K_{\perp}(\theta_{\perp}) \cdot K_{\square}(\theta_{\square}) \quad (27)$$

Equation 25 then simplifies to the following

$$\eta_{opt} = \eta_{0day} \cdot K_{\square}(\theta_{\square}) \quad (28)$$

Substituting equation 28 into equation 23 yields the following expression

$$\int_{\text{year}} E_{el} dt = \eta_{0day} \cdot K_{\square}(\theta_{\square}) \cdot \eta_{th} \cdot \eta_{pb} \cdot \dot{q}_{in} \quad (29)$$

For a constant LEC the annual cost and total cost of the plant are expressed in equation (30) and (31) respectively

$$\lambda_a = LEC \cdot \eta_{0day} \cdot K_{\square}(\theta_{\square}) \cdot \eta_{th} \cdot \eta_{pb} \cdot \dot{q}_{in} \quad (30)$$

$$\lambda_{total} = \frac{LEC \cdot \eta_{0day} \cdot K_{\square}(\theta_{\square}) \cdot \eta_{th} \cdot \eta_{pb} \cdot \dot{q}_{in}}{\kappa_a + \kappa_i + \kappa_{O\&M}} = C \cdot \eta_{0day} \quad (31)$$

It was assumed that all costing and efficiency parameters remain the same, therefore equation 31 could be simplified to a linear function. Mertins' (2009) reported the annual optical efficiency as 0.362. Using a similar SolTrace simulation for sun elevation angles from 0-65° on an ideal summer's day the day optical efficiency for the field described in Mertins' thesis was determined to be 0.54.

This creates a direct relationship between cost and nominal optical efficiency, as illustrated in Fig. 16. The area under the curve indicates designs that will be cost effective due to the proportional increase of efficiency being larger than that of the increase in cost. This means that electricity produced could be sold at a profit. Therefore, for a given nominal optical efficiency, one can find the allowable cost of the plant and use it as a constraint.

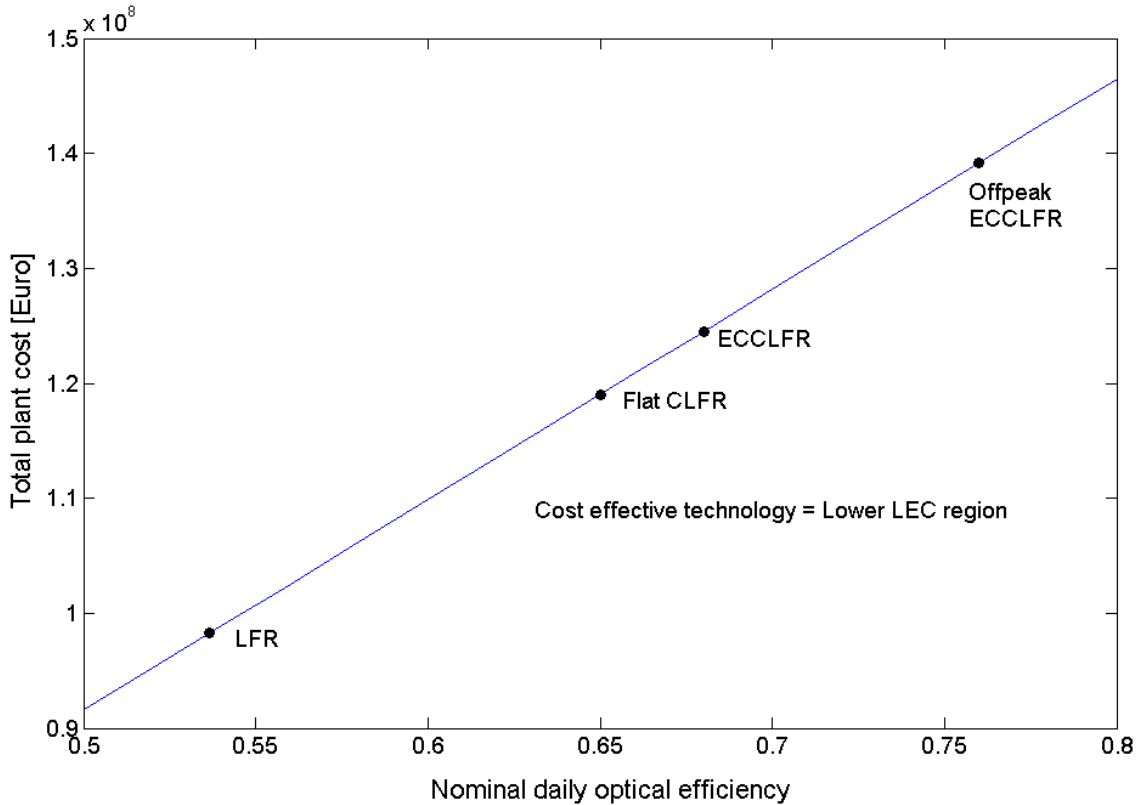


Fig. 16. Maximum total plant cost versus nominal daily optical efficiency for a constant levelized cost of electricity of LEC = 0.167 €/kWh based on a standard LFR plant costing model (Mertin, 2009)

The maximum allowable total plant cost for each model is illustrated in Table 7. The total plant costs were expressed as percentage increases to give a value that is independent of the specific costs at the

time of Mertin's original Standard LFR study (2009). The original standard LFR field was a 50MW plant. Due to the increased nominal optical efficiency, the other plant configurations will produce more electricity, thus offsetting the increased plant cost. In order to establish whether the different configurations would be able to produce 50MW power at a cheaper LEC, one would need the proposed increase in costs and the number of operating hours in the year. However, it can be seen that there was a large allowable increase in cost, especially for the Off-peak ECCLFR, implying that it would likely be a commercially viable technology.

Table 7: Maximum allowable total plant cost for the different mirror field configurations

Model	Maximum total plant cost (million Euro)	Maximum percentage increase in funds	Yearly electrical yield kWh
Standard LFR	98.25	-	$0.73 \cdot 10^8$
Flat CLFR	119.02	21.13-	$0.88 \cdot 10^8$
Suntracking ECCLFR	124.51	26.72	$0.92 \cdot 10^8$
Offpeak ECCLFR	139.16	41.63	$1.03 \cdot 10^8$

In the case where individual actuators or motors are either too expensive or take up too much space, there are solutions that have been proposed whereby an individual drive controls multiple mirrors that can be adapted to this application. Yanqing's proposal for a stretched parabolic LFR places individual mirrors on three levels with sliders that can move the mirrors in the horizontal direction (Yanqing et al., 2016) while Sen et al. (2013) suggest that a four-bar linkage system is used. Moreover, all LFR mirrors rotate at the same speed and travel through the same angle throughout a day. If one were to track the vertical movement and rotation of each mirror, a relationship could be derived between several mirrors allowing for some sort of bar linkage mechanism, thereby simplifying the actuation. These are examples that could make the implementation of the OP-ECCLFR concept even more attractive.

4. Conclusion

In conclusion, there was significant potential for a compact linear Fresnel model to increase the optical efficiency over and above that of typical linear Fresnel fields. The sun-tracking etendue-conserving CLFR model did reach higher optical efficiencies than that of the flat CLFR, however the off-peak etendue-conserving CLFR model demonstrated much higher optical efficiencies than both flat and sun-tracking models. This was specifically due to the fact that at off-peak times it was able to capture the available incoming radiation significantly better than its counterparts. In addition to this, the levels of incident radiation between the two receivers was much more comparable than for the other models, creating another significant benefit in going some way to rectifying the thermal imbalance that occurs between the two receivers for off-peak sun times in traditional CLFR.

Moreover, for both ECCLFR models, the highest incident radiation levels were obtained for ratios between the mirrors of 1, while the flat CLFR reached highest incident radiation levels for ratios of 0.5. Equal mirrors in the central section simplifies manufacturing as all the mirrors in the field could then be of the same size.

Therefore, the ECCLFR model offers advantages optically, thermally and on a manufacturing level. It is a technology with comparatively limited research and very few commercial plants, however creating an optically efficient collector makes it a more viable competitor with parabolic trough technologies.

5. Future work

The investigations thus far have been based on performance throughout the day for an ideal summer day and Gaussian sunshape. This doesn't account for seasonal DNI variation or DNI variation on non-ideal summer days and more realistic sunshapes, which would affect the annual performance of the plant. More detailed DNI models can be used to better determine annual efficiencies. Secondly, the interaction between the receiver internal geometry and the collector should be investigated, as this impacts the amount of radiation that is ultimately absorbed by the receiver.

Acknowledgements

The authors would like to acknowledge the support of the University of Pretoria (South Africa) and the South African National Research Foundation (DST-NRF Solar Spoke).

References

- Abbas, R., Martinez-Val, J.M., 2015. Analytic optical design of linear Fresnel collectors with variable widths and shifts of mirrors. *Renew. Energy* 75, 81-92
- Ardekani, M.M., 2017. Optical, thermal and economic optimization of a Linear Fresnel Collector. PhD thesis, University of Pretoria
- Bendt, P., Rabl, A., Gaul, H.W., Reed, K.A., 1979. Optical Analysis and Optimization of Line Focus Solar Collectors. Solar Energy Research Institute SERI task number 3432.30
- Chaves, J., Collares Pereira, M., 2010. Etendue-matched two-stage concentrators with multiple receivers. *Sol. Energy* 84, 196-207
- Chaves, J., 2016. Introduction to Nonimaging optics. Second Edition. Taylor & Francis Group
- Eck, M., Hirsch, T., Feldhoff, J.F., Kretschmann, D., Dersch, J., Gavilan Morales, A., Gonzalez-Martinez, L., Bachelier, C., Platzer, W., Riffelmann, K.J., Wagner, M., 2014. Guidelines for CSP yield analysis – optical losses of line focussing systems; definitions, sensitivity analysis and modelling approaches. In: Presented at SolarPACES 2013, Las Vegas, United States of America. *Energy Procedia* 49, 1318-1327.
- Ford, G., 2008. CSP: bright future for linear fresnel technology? *Renewable Energy Focus* September/October, 49-51.
- Häberle, A., Zahler, C., Lerchenmuller, H., Mertins, M., Wittwer, C. Trieb, F., Dersch, J., 2002. The solarmundo line focussing Fresnel collector: optical and thermal performance and cost calculations. In: Presented at 11th SolarPACES International Symposium, Zurich, Switzerland.
- Hertel, J.D., Martinez-Moll, V., Pujol-Nadal, R., 2015. Estimation of the influence of different incidence angle modifier models on the biaxial factorization approach. *Energy Conversion and Management* 106, 249-259.
- McIntire, W.R., 1982. Factored Approximations for Biaxial Incident Angle Modifiers. *Sol. Energy* 29, 315-322
- Mertins, M., 2009. Technische und wirtschaftliche analyse von horizontalen Fresnel-kollektoren PhD thesis. University of Karlsruhe, In German.
- Mills, R.M., Morrison, G.L., 1999. Compact Linear Fresnel Reflector Solar Thermal Powerplants. *Sol. Energy* 68, 263-283.
- Moghimi, M.A., Craig, K.J. and Meyer, J.P., 2017. Simulation-based optimisation of a linear Fresnel collector mirror field and receiver for optical, thermal and economic performance. *Sol. Energy* 153, 655-678.
- Muller-Steinhagen, H., Trieb, F., Trieb, F., 2011. Concentrating solar power; A review of the technology. Institute of Technical Thermodynamics, German Aerospace Center, Stuttgart, Germany
- Rungasamy, A.E., Craig K.J., Meyer J.P., 2015. 3-D CFD modeling of a slanted receiver in a compact linear Fresnel plant with etendue-matched mirror field. In: Presented at SolarPACES 2014, Beijing, China. *Energy Procedia* 69 188-197.

- Sen, P.K., Ashutosh, K., Bhuwanesh, K., Engineer, Z., Hegde, S., Sen, P.V., Davies, P., 2013. Linear Fresnel mirror solar concentrator with tracking. In: Presented at the 5th BSME International Conference on Thermal Engineering. *Procedia Engineering* 56, 613-618
- Wendelin, T., Dobos, A., 2013. SolTrace: A Ray-Tracing Code for Complex Solar Optical Systems. Technical report NREL/Tp-5500-59163
- Yanqing, Z., Jifu, S., Yujian, L., Leilei, W., Qizhang, H., Gang, X., 2016. Design and experimental investigation of a stretched parabolic linear Fresnel reflector collecting system. *Energy Conversion and Management* 126, 89-98.